

Submarine slides north of Puerto Rico and their tsunami potential

Uri ten Brink (*U.S. Geological Survey, Woods Hole, MA 02543; utenbrink@usgs.gov*)

Eric L. Geist (*U.S. Geological Survey, Menlo Park, CA 94025; egeist@usgs.gov*)

Patrick Lynett (*Texas A&M University, College Station, TX 77843;*

plynett@civil.tamu.edu)

Brian Andrews (*U.S. Geological Survey, Woods Hole, MA 02543; bandrews@usgs.gov*)

New multibeam bathymetry of the entire Puerto Rico trench reveals numerous retrograde slope failures at various scales at the edge of the carbonate platform north of Puerto Rico and the Virgin Islands. The slumped material comprises carbonate blocks, which fail, at least in initial stages, as a coherent rock mass. This, combined with the fact that the edge of the carbonate platform is steeper than most continental slopes, indicates a higher potential for run-up than along many other U.S. coasts. The style of slope failure appears to be rock falls, slide blocks and debris avalanches. Secondary failure of the failed carbonate products and of the underlying forearc sediments and rocks may lead to debris flows and turbidity flows. Fissures, discovered in the ocean floor near the edge of the platform, indicate that the process is expected to continue in the future. One of the slope failures, the Arecibo amphitheater, previously thought to represent a single giant slide with a volume of 900-1500 cu. km, appears to comprise smaller failures. The expected maximum tsunami run-up on the northern coast of Puerto Rico from one of these slope failures is <20 m, much lower than previously estimated. A recurrence rate of 100s ky was calculated for the largest observed failures along the edge of the carbonate platform north of Puerto Rico using simple assumptions. Smaller landslides would presumably occur at a higher recurrence rate. Elsewhere around the island, a 20-km wide failure scarp was discovered in the Upper Mona rift and could be associated with the 1918 tsunami and earthquake that hit northwestern Puerto Rico. Large slope failures were also discovered for the first time on the northern side of the Puerto Rico trench. Because Puerto Rico trench slides occur at large water depths (~6000 m), have large horizontal and vertical dimensions, and the directivity from tsunamis emanating from these slides is toward Puerto Rico, they may be of particular concern and may necessitate further study.

1. Introduction

Evidence for tsunamis generated by submarine slope failures has been accumulating during the past decade (e.g., [Ward, 2001]). The highly destructive 1998 Papua New Guinea tsunami, for example, was likely amplified in the near field by a landslide-generated tsunami, in addition to the seismogenic tsunami [Satake and Tanioka, 2003]. Tsunamis generated by submarine slope failures have only a local effect, because relatively high-frequency waves are being excited by the slides and these high frequencies attenuate quickly with distance from the source [Ward, 2001]. However, they can strike with little warning, because of the proximity of the tsunami source to the affected coast and because ground shaking that triggers offshore landslides may be small or lacking. Hence, it may not be possible to provide civil defense authorities with adequate tsunami warning from submarine slides. A better strategy in this case would be to mitigate the hazard by identifying vulnerable coastal regions and modifying their usage, and by educating the public. Numerical simulations of landslides

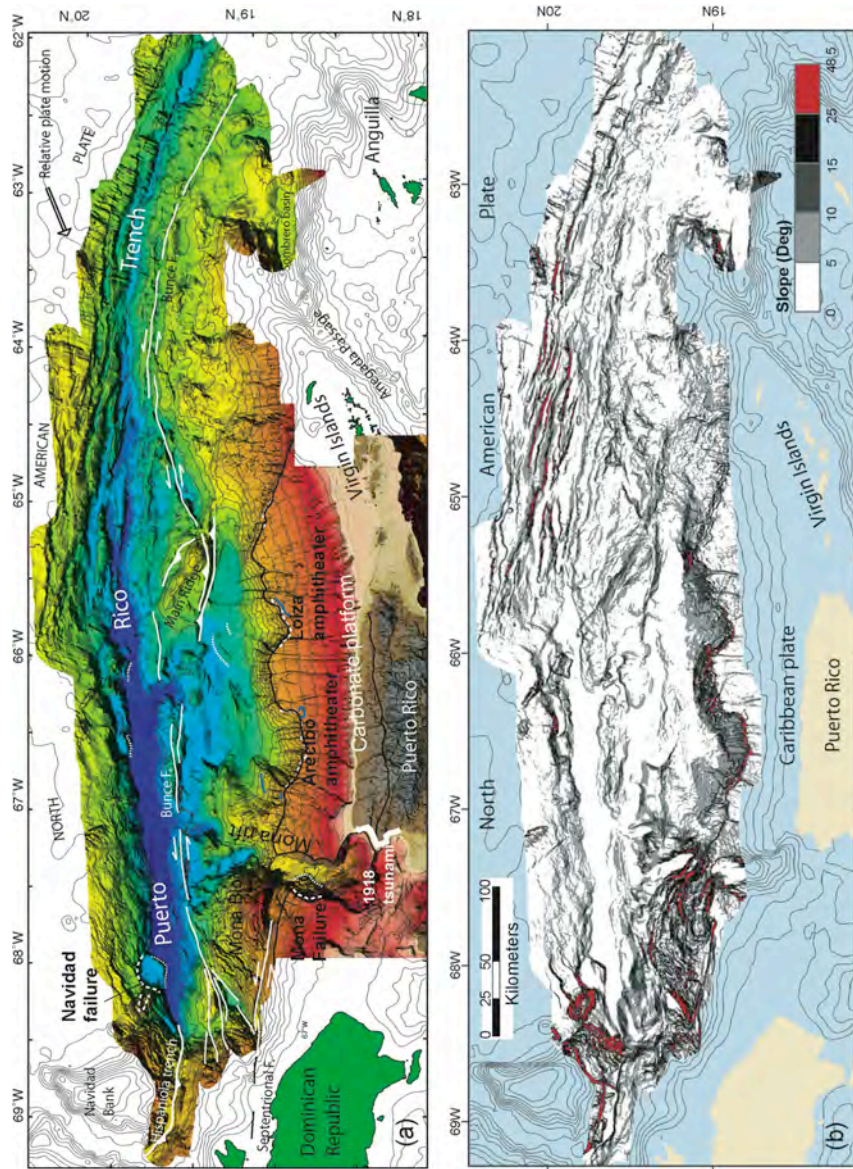


Figure 1. (a) Bathymetric map of the Puerto Rico trench and its vicinity from our new multibeam sonar survey [ten Brink *et al.*, 2004a], single-beam bathymetry compilation around Puerto Rico (A. Mercado, written communication, 2003), LIDAR data near shore (J. Brock, written communication, 2003), and topography of Puerto Rico. Contour interval is 500 m. Barbed white lines – thrust faults; white line – strike-slip fault; heavy black line – northern edge of tilted carbonate platform and southern edge on land; dashed lines – head scarp of slope failures; dotted line – possible debris toe; blue lines – fissures in the sea floor. (b) Map of the slope angle (in degrees) of the bathymetry of the

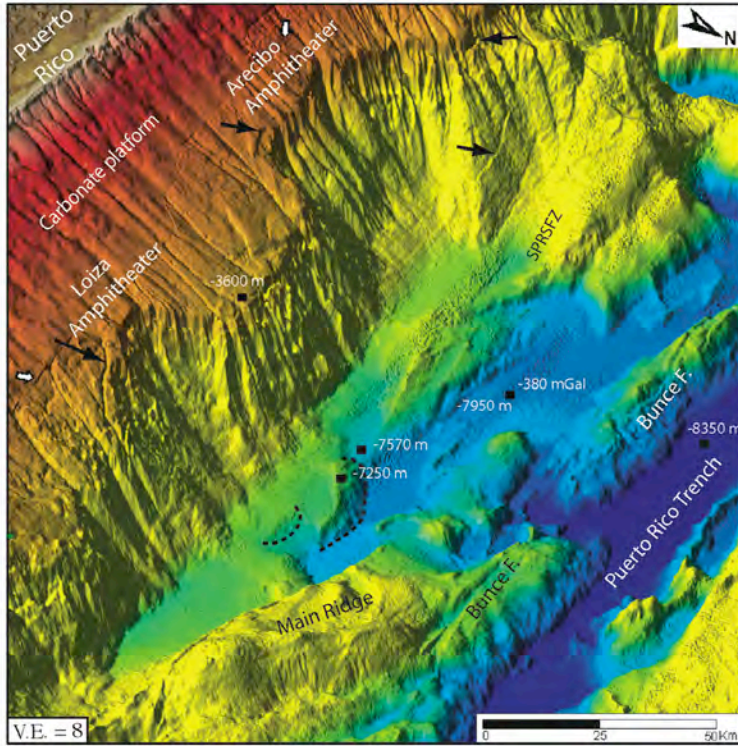
Puerto Rico trench. The slope was calculated as the maximum horizontal slope on a grid interval of 300 m. A finer grid interval will produce higher slope angles. Thin contours – bathymetry from ETOPO2 at 500 m intervals.

tsunamis and their run-up on shore can help identify these vulnerable coastal regions. Realistic simulations, however must rely on a good knowledge of potential sources, a good knowledge of the bathymetry, and an understanding of the style of slope failure.

The region north of Puerto Rico may pose significant tsunami hazards to Puerto Rico, the Virgin Islands, and the Dominican Republic. A tsunami killed 40 people in NW Puerto Rico following a magnitude 7.3 earthquake in 1918 [Mercado and McCann, 1998]. Large landslide escarpments have been mapped on the seafloor north of Puerto Rico [Grindlay, 1998; Schwab *et al.*, 1991], although their ages are unknown. One of the escarpments, the Arecibo Amphitheater, was simulated as a single failure with run-up on the north shore of Puerto Rico possibly reaching 55 m [Mercado *et al.*, 2002]. In this paper we use multibeam bathymetry [ten Brink *et al.*, 2004a] and re-processed seismic reflection profiles to describe and quantify slope failures and to identify sites of potential future failures. The data indicate that slope failure is likely an incremental process even within the amphitheater. A numerical simulation for landslide-generated tsunami is presented for the north coast of Puerto Rico from one such failure in the Arecibo Amphitheater and indicates a run-up height only 1/3 of the previous estimate.

2. Background

The Puerto Rico trench is a subduction zone, where the North American (NOAM) plate is subducting under the Caribbean plate (Figure 1). Subduction is highly oblique (10° - 20°) to the trench axis with a large component of left-lateral strike slip motion [ten Brink *et al.*, 2004b]. In addition to its extremely deep seafloor, the Puerto Rico trench is also characterized by the most negative free-air gravity anomaly on Earth, -380 mGal, which indicates a dynamic departure from isostatic equilibrium. It is unclear, however, whether the trench continues to subside or whether subsidence has recently ended, and the trench has not yet filled with sediment. Subsidence of the trench probably caused the north shore of Puerto Rico and its offshore region, which are covered by carbonate rocks to tilt northward. The carbonate platform was horizontally deposited over Cretaceous to Paleocene arc rocks starting in the Late Oligocene. Then, at 3.3 Ma or later, the carbonate platform was tilted by 4° toward the trench such that its northern edge is at a depth of 4000 m and its reconstructed elevation on land in Puerto Rico is at +1300 m ([ten Brink, in press]; Figures 1, 2a). The tilting



(a)

(b)

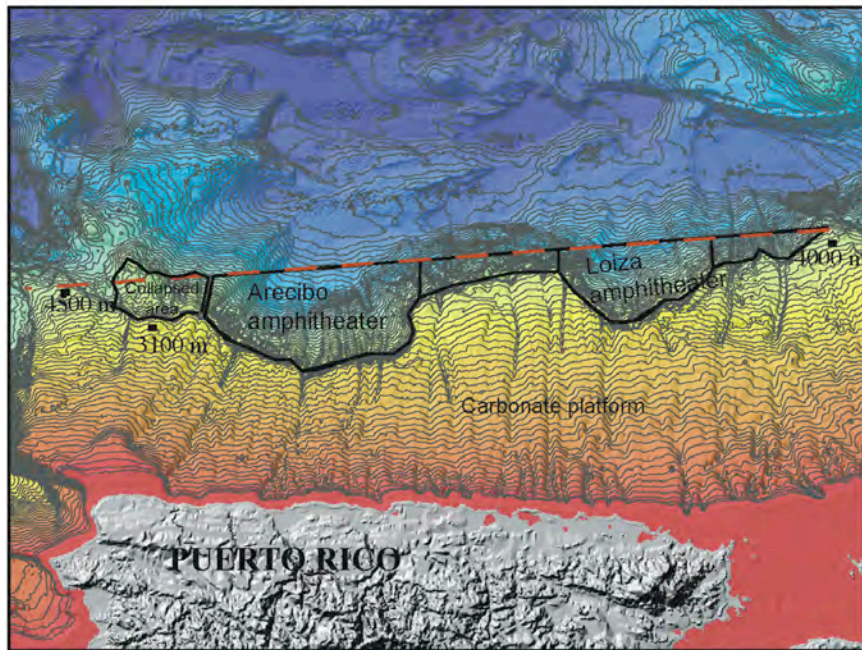


Figure 2. (a) Perspective view of the edge of the carbonate platform. Viewing direction is from the NE to the SW. White arrows point to the boundary between multibeam bathymetry and single-beam bathymetry. Black arrows point to fissures in the seafloor. Dotted lines are debris toes. The locations of a previously suggested strike-slip fault (SPRSFZ) and the largest free-air gravity anomaly on Earth (-380 mGal) are shown. Stippled textures (e.g., near SPRSFZ) are multibeam acquisition artifacts. (b) Bathymetry of the northern edge of the carbonate platform contoured at 100 m interval. The estimated edge of the platform before failure started is shown as a straight line located where a northward extension of the carbonate platform tilted at 5° would lie at a depth of 4500 m. The total estimated eroded area enclosed by black lines is 2120 km², and the total areas of the Arecibo and Loiza amphitheatres is 1147 and 692 km², respectively.

episode may have been very short, less than 40 ky, [ten Brink, in press]. The subsidence and tilting have probably created gravitational instabilities and steep topographic slopes (Figure 1b), which are vulnerable to slope failures, particularly during earthquakes. Other tectonic motions, such as the opening of Mona Passage, the subduction of Main Ridge, and the subduction of the North American plate, continue to shape the area and can generate earthquakes that promote slope failure.

The 770-km long Puerto Rico trench from the Dominican Republic in the west to Anguilla in the east was mapped with multibeam sonar during three cruises in 2002 and 2003 [ten Brink *et al.*, 2004a]. Parts of the Puerto Rico trench were previously surveyed with side scan sonar [Grindlay *et al.*, 1997; Scanlon and Masson, 1996; Schwab *et al.*, 1991] and multibeam bathymetry [Dillon *et al.*, 1998] often at lower resolution and with line orientation and spacing that did not provide complete bathymetric coverage. The data, presented here, were collected using the SeaBeam 2112 multibeam sonar system aboard the NOAA ship Ron Brown with sufficient swath overlap and proper line orientation for hydrographic survey. The data were gridded at 150 m grid size following resolution tests and at 50 m grid size at depths smaller than 4000 m. Vertical resolution is estimated to be 0.5-1% of the water depth (10-80 m; L. Mayer, oral comm., 2003). Backscatter mosaic images derived from the multibeam bathymetry data aided in the interpretation. The total mapped area with multibeam sonar is 100,000 km² (Figure 1). Seismic profiles from the University of Texas Seismic data center (<http://www.ig.utexas.edu/sdc>) were migrated in time using the Stolt post-stack migration algorithm and provided vertical cross-section of some of the slope failures. We focus our discussion on three areas: The northern edge of the tilted carbonate platform, the Mona Rift, and the downgoing North American plate north of the trench (Figure 1).

3. The northern edge of the carbonate platform

The northern edge of the carbonate platform north of Puerto Rico is characterized by two large amphitheater-shaped headwall scarps, the Arecibo amphitheater 37 km north of Arecibo, Puerto Rico [Mercado *et al.*, 2002; Scanlon and Masson, 1996; Schwab *et al.*, 1991] which is 50-km across, and the Loiza amphitheater, 48 km north of Loiza, Puerto Rico [Scanlon and Masson, 1996], which is 35-km across (Figures 2 and 3). Smaller failures are observed adjacent to these amphitheaters, and the westernmost edge of the platform appears to have collapsed but was translated very little. Several smaller scarps and slope failures were also identified all along the edge of the carbonate platform (Figures 2 and 3).

3.1 Loiza amphitheater

The backscatter image (Figure 3b) shows high reflectivity in the western half of the Loiza amphitheater, and lower reflectivity on the eastern side. The high reflectivity region extends downward into the abyssal plain and ends in a low hill (Figure 3a). We interpret this hill to be the toe of a debris field, which extended about 40 km from the head of the scarp. Seismic profile 1a across the failure scarp and the debris field has a classic concave shape (Figure 4a). The debris field itself is elevated by 40-50 m above the surrounding area, barely above the vertical resolution of our data. A layer of debris 200-250 msec thick can perhaps be identified on the seismic profile (Figure 4a). In contrast, the eastern sector of the amphitheater has low reflectivity. The part of seismic profile 7 (Figure 4b), which is below 6.5 s two-way travel time (TWTT), crosses the eastern sector obliquely and shows a hummocky surface and irregular reflectors. This sector of the amphitheater is interpreted to represent a series of smaller failures along the slope.

We propose that slope regions of high back scatter (such as failure A in Figure 3b) may be associated with a large debris flow over the slope, which has not yet been modified by secondary failure and may be relatively recent. Although high back scatter also results from sediment discharge along channels in the inclined carbonate platform, these narrow channels are clearly distinct from the slope reflectivity and they mostly terminate at the carbonate platform edge.

A 15-km long, several hundred meters wide and at least 100 m deep fissure runs at a distance of 2-5 km above the eastern headwall scarp of the Loiza Amphitheater (Figures 3a and 3c). The fissure cuts obliquely to the slope of the carbonate platform, suggesting that it was not developed as subterranean drainage in the limestone layers. More likely, it represents an extension normal

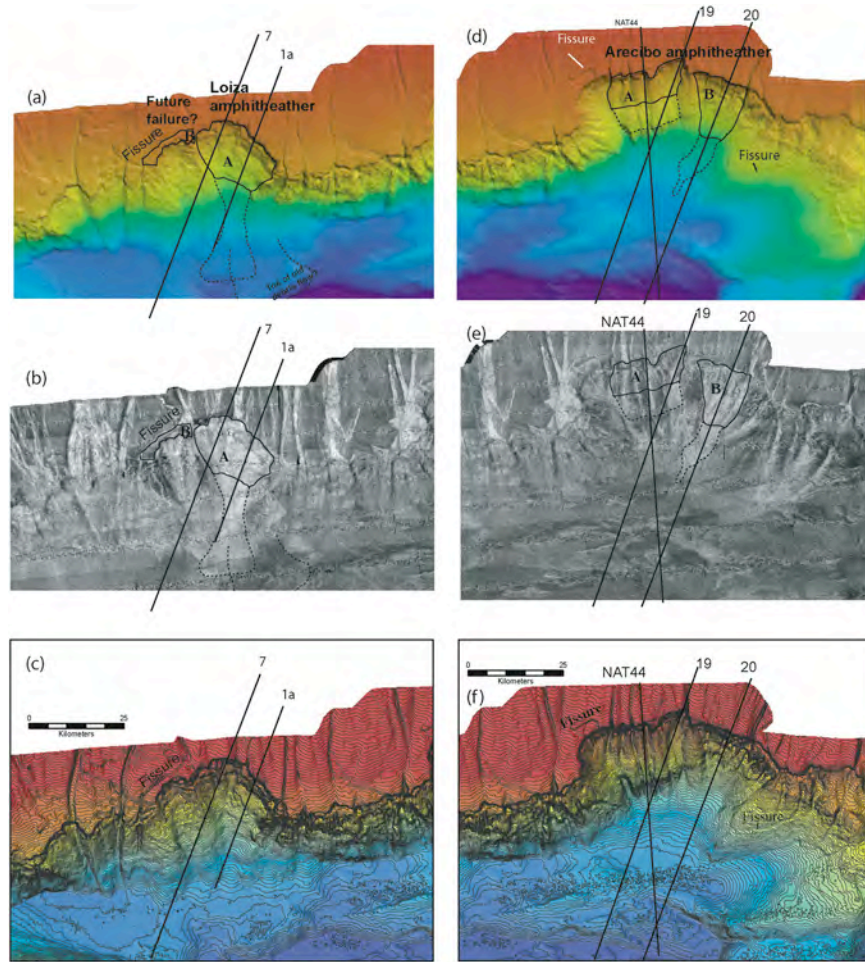


Figure 3 (a) View of the Loiza Amphitheater and the edge of the carbonate platform. Solid lines are locations of bathymetric profiles shown in Figure 4. Area A, which is enclosed by a solid line is an interpreted slope failure, which produced the debris flow enclosed by a dashed line with a debris toe. Area B is a hypothesized area that would slide should the fissure SE of the headwall of the escarpment continue to open. Dashed line marked by 3 is a suggested old toe of a debris avalanche. (c) Backscatter image of the map shown in (a). Profiles and solid and dashed lines are as in (a). High reflectivity represents debris flow from Failure A and turbidity flows along the drainage gullies coming of the carbonate platform. (c) Contour map of Loiza Amphitheater and its vicinity. Contour interval is 50 m. Note the large fissure SE of the headwall, numerous other small failures outside the amphitheater. (d) View of the Arcibo Amphitheater and the edge of the carbonate platform. Solid lines are locations of bathymetric profiles shown in Figure 4. Area A enclosed by a solid line is interpreted as a rotational slide whose debris, enclosed by a dashed line that is perched on the lower slope. Area B enclosed by a solid line is interpreted as another slope failure, which produced the debris flow enclosed by a dashed line. (e) Backscatter image of the map shown in (d). Profiles and solid and dashed lines are as in (d). High reflectivity represents debris flow from slide B and turbidity flows along the drainage gullies coming of the carbonate platform. (f) Contour map of

Arecibo Amphitheater and its vicinity. Contour interval is 50 m. Note the lack of debris toes at the base of the slope. Wiggly contours on a small scale are due to acquisition artifacts.

to the steep ($\leq 45^\circ$) headwall of the amphitheater because of the horizontal tensile stresses that develop in an unsupported wall. If this interpretation is correct, then another future failure (marked B in Figure 3a), may take place, and depending on its acceleration, it may generate tsunami waves that will propagate toward the Virgin Islands.

A 300 m high and 25 km long ridge in the abyssal plane may be an old toe of a debris flow (Figure 3A) although a seismic profile, oriented obliquely to this ridge does not show a clear internal structure. If this ridge were a debris toe, it would have originated from an older failure on the eastern side of the Loiza Amphitheater, which was moving in a NW direction prior to the occurrence of Failure A.

3.2 Arecibo amphitheater

The Arecibo amphitheater also appears to have been formed by several slope failure events. The amphitheater-shaped scar was previously postulated to have formed by a giant submarine slope failure with a displaced volume of over 910-1500 km³ [Grindlay, 1998; Schwab *et al.*, 1991]. Maximum run-up of 30-55 m was calculated from this failure, with a run-up >10 m along the entire northern coast of Puerto Rico [Mercado *et al.*, 2002]. The backscatter image shows high reflectivity within the funnel-shaped area of high reflectivity on the western side (marked B in Figure 3e) of the amphitheater, which perhaps represents debris or turbidity flow. The cross-section of the area of high reflectivity area (Seismic profile 20 (Figure 4c) is concave (with the exception of the upper slope above 6.5 sec.), similar to the shape of the reflective slope failure A in the Loiza Amphitheater (Figure 4a).

The eastern amphitheater slope is much less reflective with the exception of narrow bands that can be traced to the drainage system higher up on the carbonate platform (Figure 3e). The slope in this region is probably the result of a rotational slide, where the upper slope slid about 8 km and the debris is perched on the lower slope (Figures 3f and 4d and 4e). The seismic stratigraphy on the slope shows remarkably coherent reflections suggesting that carbonate blocks slid coherently. The lower slope is steep and appears to be eroded by retrograde gullies (Figure 3f).

The abyssal plain in front of the Arecibo Amphitheater is 150-200 m shallower than the base of the slope east of the Arecibo amphitheater (Figure 2b and 3f),

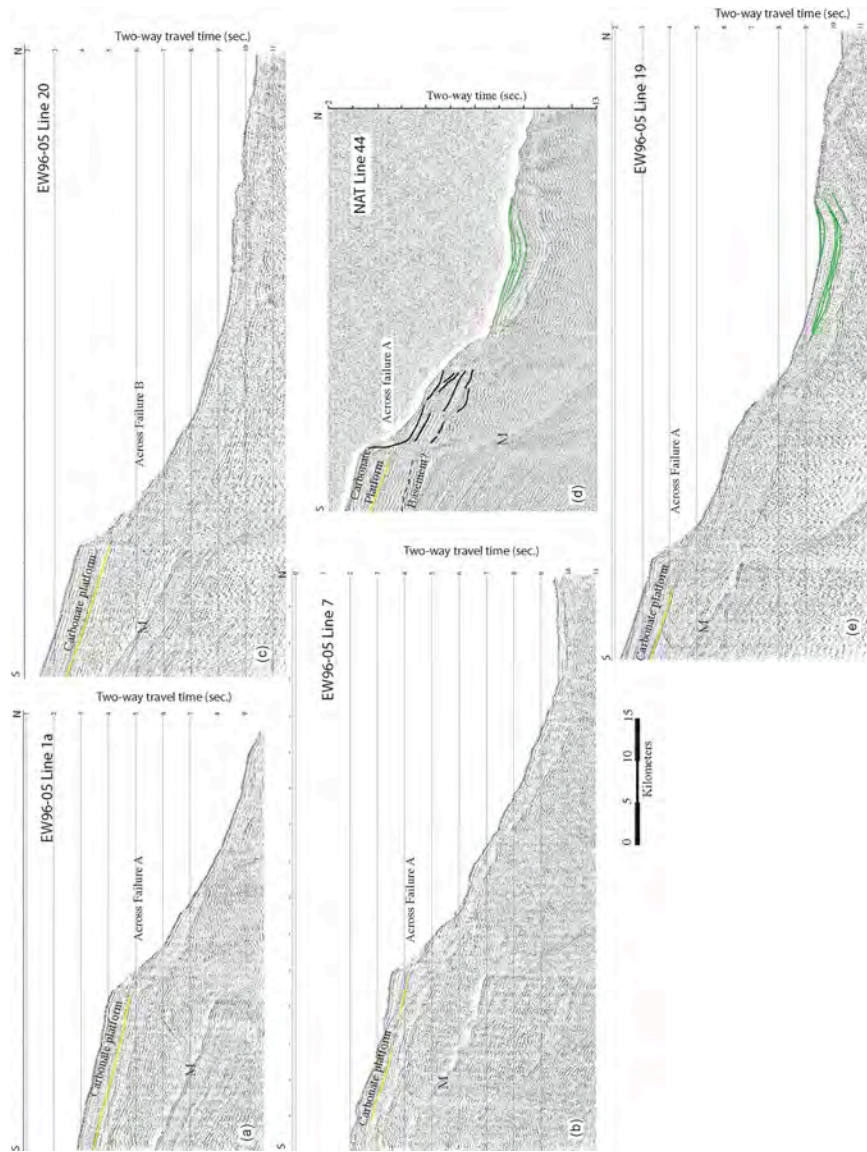


Figure 4. Reprocessed seismic reflection profiles (a and b) across the Loiza and (c, d, and e) the Arecibo amphitheater. See Figure 3 for location. Note that profiles 7 and 19 are oriented oblique to the slope. All the profiles, with the exception of (d) are single-channel profiles. All the profiles were migrated using the Stolt migration, filtered, and gained. Yellow – interpreted bottom of the carbonate platform. Green – interpreted boundaries between sequences of turbidity flows. M – water bottom multiple.

perhaps because more sediment was deposited in front of the amphitheater than to the east. The abyssal plain is underlain by up to 2 s TWTT or over one km thick packet of sediments that dip and thicken to the north (Figure 3c, 3d, and 3e). Grindlay [1998] interpreted this sedimentary packet to be turbidities from the major slumping event that created the Arecibo amphitheater, but the internal stratigraphy indicates several distinct sedimentary packet, which were probably deposited during different failure events, or during massive sediment run-offs from the Puerto Rico after heavy storms.

A 7x3 km area along the eastern headwall of the Arecibo amphitheater appears to be surrounded by fissures (Figure 3d) and to be up to 200 m lower than the surrounding carbonate platform (Figure 3f). This may be an indication of the beginning of a new slope failure of part of the Arecibo amphitheater.

3.3 *Mona rift*

A 20-km-long section of the western wall of the upper Mona Rift is scoured by a slope failure (Figures 5a and 5b). The headwall varies in height from 1250-3350 m below sea level. The failure scarp appears in map view to be <5 km wide and the debris field ahead of it is 2.5-10 km wide. In side view (Figure 5a), the failure appears almost as a rock fall. A cross-section of the failure (Figure 5c and d) shows an 11-km-long by 0.5 thick blocky section of debris field. The debris field is interpreted as a combination of rock fall and debris avalanche. Using seismic velocity of 2 km/s for the debris field and 2.75 km/s for the carbonate platform at the headwall [*van Gestel et al.*, 1998], the area of the debris field is the equivalent of a 4.1 km wide section of failed platform. The failure appears to be recent because the debris field comprises of discrete blocks and because does not cover the most recent sediments filling the rift.

The upper Mona rift (Figure 1a, 5a and b) cuts across the carbonate platform north of Puerto Rico. The rift walls are very steep (>25°) and are likely normal fault planes along which east-west extension between the Puerto Rico and the Hispaniola blocks [*Mann et al.*, 2002] takes place. The tsunami of 1918 which killed 40 people along the termination of the rift at the northwestern shore of Puerto Rico, probably initiated at the upper Mona rift [*Mercado and McCann*, 1998]. The tsunami followed almost immediately a magnitude 7.3 earthquake which caused extensive damage and additional 76 fatalities in NW Puerto Rico (*ibid.*). Eyewitness account (quoted in [*Mercado and McCann*, 1998]) described the sea receding before it returned to flood the shore with waves up to 6 m high. This indicates that the downward motion along the normal fault, on which the earthquake had likely occurred, was directed away from shore. Mercado and

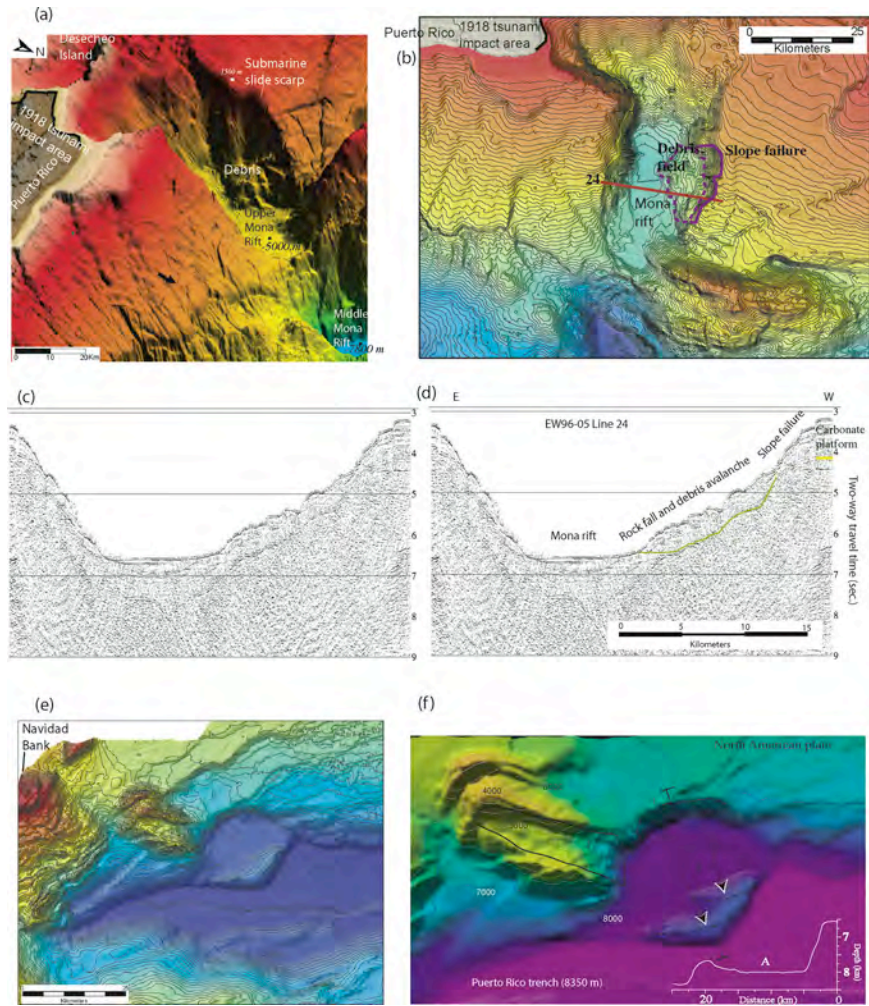


Figure 5. (a) Side view of the slide in the upper Mona rift. Back arrow marks the boundary between our higher resolution multibeam bathymetry data and the existing bathymetry compilation from single beam bathymetry (A. Mercado, written communication, 2002). (b) Contour map of the Upper Mona Rift. Contour interval is 100 m. Black arrow is as in (a). Solid line is the estimated area of the slide and dashed line is the estimated area of the debris field. Red line is the location of the profile in (c) and (d). (c) Seismic profile 24 across Mona failure. See Figure caption 4 for details of the processing sequence. (d) Interpretation of the seismic profile. (e) Bathymetric map of the Navidad Bank area. See Figure 1 for location. Contour interval is 100 m. There may be numerous slides on the slope of Navidad Bank that faces the Puerto Rico trench. (f) Bathymetric map of the largest failure east of Navidad Bank. Solid line labeled 1 perhaps encloses the slide area although there appear to be two debris toes, indicating perhaps repeated failure along the same escarpment. Dashed line A marks the location of the profile in the inset. Solid line labeled 2 is perhaps another landslide that scooped part of the seamount.

McCann (1998) therefore located the fault along the eastern wall of the rift. Alternatively, Figure 5b shows that the slide scarp is curved toward the SW and therefore, the motion of the slide was perhaps directed to the northeast. A more accurate bathymetry of the shallower section of Mona rift is needed together with numerical simulations to determine what impact tsunamis generated from Mona rift slides has on the neighboring islands.

3.4 Northern side of the trench

Slope failures are not limited to the carbonate platform north of Puerto Rico. Several scarps and deposits were observed in the multibeam bathymetry for the first time on the northern trench wall, where the North America plate drops into the trench by 2-2.5 km over a distance of 20-25 km. The largest scarp, located at a depth of 6500 m is 20-km wide and 1500-m high and a 600 m high mound 15 km in front of the scarp presumably is the deposit derived from the scarp (Figure 5f). The mound has two parts, which indicates that the failure occurred as at least two separate events. The circular region between the scarp and the toe is 300 m higher than the floor of the trench, and is likely filled with the products of the slope failures. There are no seismic profiles across this region to determine whether it is filled with debris avalanche or turbidity flows. The backscatter image shows low reflectivity from the scarp to the toe, with the exception of the area located within 5 km of the base of the scarp, perhaps because the failures are older and a veneer of pelagic sediments has covered their products.

The areas to the north and the west of that scarp, including what appears to be an excavated side of a seamount may also be associated with submarine slope failures. Slopes reaching 45° and vertical offsets of up to 8 km were also observed near Navidad Bank and Mona Block (Figure 1a), and along fault scarps on the descending NOAM plate NE of the Virgin Islands. These conditions may generate submarine slope failures. Slope failures on the northern wall of the trench should be evaluated for tsunami potential because the direction of slide movement and therefore the directivity of slide-generated waves are toward Puerto Rico.

4. Characteristics of slope failures around the Puerto Rico trench

Bathymetric slopes reaching 45° can be found along the northern edge of the Carbonate platform north of Puerto Rico, along the walls of the Upper and Middle Mona rift basins, around Mona block, along the eastern end of Septentrional Fault, around Navidad Bank, and along the descending NOAM plate north of the trench (Figure 1). Many landslide scarps along the Atlantic

and Pacific margins of North America and in the Gulf of Mexico are, on the other hand, found on much smaller slope angles (as small as 0.5° , [Prior and Coleman, 1984]). The slope failures, which they represent, are thought to be induced by rapid sedimentation and tectonic activity, causing the slope to become steeper, and by elevated pore pressure, gas pressure, wave generated or tidal generated bottom pressure (e.g., [Driscoll et al., 2000; Locat et al., 2004; Prior and Coleman, 1984]).

The edge of the continental shelf along much of North America is covered with clastic sediments, which in high sedimentation areas may be unconsolidated. (The exceptions are the Blake Escarpment and the exposed lower continental slope from Florida to New Jersey, which are made of limestone and chalk [Dillon et al., 1993; Twitchell et al., 1993], and may be analogous to the Puerto Rico margin.) When the slope fails, these sediments may disintegrate into debris flows and a turbidity current, such as may have happened in the 1929 Grand Bank event [Piper et al., 1999]. By contrast, slope failure around Puerto Rico involves either carbonate layers or oceanic crust. The north coast of Puerto Rico and the area surrounding the Upper Mona Rift are covered by an average of 1600 m thick layer of carbonate rocks (mostly limestone) [van Gestel et al., 1998], which will tend to fail as a coherent rather than internally deformable rock mass. Navidad Bank is covered by several km of carbonate rocks [Freeman-Lynde and Ryan, 1987]. In all these areas we expect slope failure to occur as rock falls, block and debris slides, and to a lesser extent, debris avalanches, and debris flows (cf., Varnes, 1978). These failure modes are indeed observed in the multibeam imagery and seismic profiles, for example, Arecibo Failure A (Figures 3d, 4e and 4f) and Mona rift (Figures 5a and 5d).

The carbonate platform comprises a 1-2 km thick layer of highly massive or layered limestone, with some shales and shaly sandstone toward the bottom of the section (the San Sebastian Formation)[Monroe, 1980; van Gestel et al., 1999]. It is underlain by volcanoclastic, volcanic, and igneous rocks of the arc and forearc, which may be less coherent during failure. The carbonate layer may act as a cap that protects the underlying less coherent layers from failing (Figure 4). When part of this cap detaches from the rest of the platform and either rotates (Figure 4d) or disintegrates (Figure 4a), it exposes the underlying layers to further failures, probably in the form of smaller more incremental events (e.g., Figure 4b). A carbonate block may detach from the platform by a combination of vertical fissures, in which carbonate dissolution may take place, and reduced basal friction on basal shale and clay layers. The fissures must be oriented subparallel to the edge of the platform to allow the blocks to detach, and the

carbonate dissolution is probably aided by fresh water runoff from the island. The process may therefore be limited by the rate at which these fissures can form and cut through the entire thickness of the carbonate layer.

Slope failures off Navidad Bank, Mona Block, and the walls of Mona rift are likely made of thick coherent limestone blocks. Slope failures on the NOAM plate are likely to comprise about 500 m of pelagic sediment and chert layers underlain by upper oceanic crust basalts, and these failures may develop differently than those along the carbonate platform.

The failure of coherent blocks on a steep slope appears to cause a high tsunami run-up. The 1992 Flores Island tsunami was accompanied by slope failures in the surrounding carbonate reef and generated a maximum run-up of 26 m [Imamura *et al.*, 1995], however, the submarine portion of the slide has not been mapped. The collapse of the Ritter Island volcano in 1888, which was associated with sliding of coherent blocks, had produced a maximum run-up of at least 15 m [Ward and Day, 2003]. The 1975 Kalapana earthquake in Hawaii was argued by some authors to be the result of a coherent slope failure of the flank of Kilauea volcano (e.g., [Ma *et al.*, 1999]) and it produced a maximum run-up of 15 m. While it appears that failure of coherent blocks on a steep slope may generate a high tsunami run-up, there is no evidence to suggest that the opposite is also true, namely, that the failure of less coherent blocks on lower slopes will generate small tsunamis. The 1929 Grand Banks tsunami with a maximum run-up of 13 m was triggered by a M=7.2 earthquake, and was probably amplified by large-scale slope failure and turbidity flow ([Piper *et al.*, 1999; Hughes Clark, 1990), but the exact contribution of the slope failure to the Grand Banks run-up is unknown. Smaller scale failures such as the Palos Verde [Locat *et al.*, 2004] and Goleta [Edwards *et al.*, 1993] are prehistoric and have no known associated tsunamis.

For a slide of constant spatial dimensions, tsunami wave height is affected by the time evolution and terminal speed of the slide. These dynamic properties, in turn, depend on a complex interplay of forces (e.g., basal friction and drag) and physical properties (e.g., friction coefficient along joints and fractures) for coherent slides of the type studied here. (For comparable analysis of deformable slides, see Locat *et al.* [2004]) When performing the coupled landslide motion – hydrodynamic simulations, the impact of these factors on the generated tsunami is tested by systematically modifying the time duration of the slide.

5. Hydrodynamic Simulation

The effects of slope failure in the Puerto Rico trench has on the resulting tsunamis, was explored using a hydrodynamic simulation similar to that used by *Mercado et al.* (2002) for the entire Arecibo Amphitheater. A simplified representation of Failure A in the Arecibo Amphitheater (Figure 3d) is parameterized according to its effective width and total length of the slide slope in the area of evacuation (Figure 6). The dimensions of this failure are assumed to be 22 km wide (along strike) with a 3.5 km length (down-slope) of the depletion zone and a 4.5 km length of the debris field (total length 8 km). The average thickness of the slide is assumed to be approximately 1 km. The slide is then modeled as a region of depletion with a sharp head scarp and a down slope region of debris fan accumulation (cf., *Trifunac et al.*, 2003). Movement of the slide is specified according to a duration time (t_d) with smooth ramps used to simulate the accelerating (starting) and decelerating (stopping) phases of slide motion.

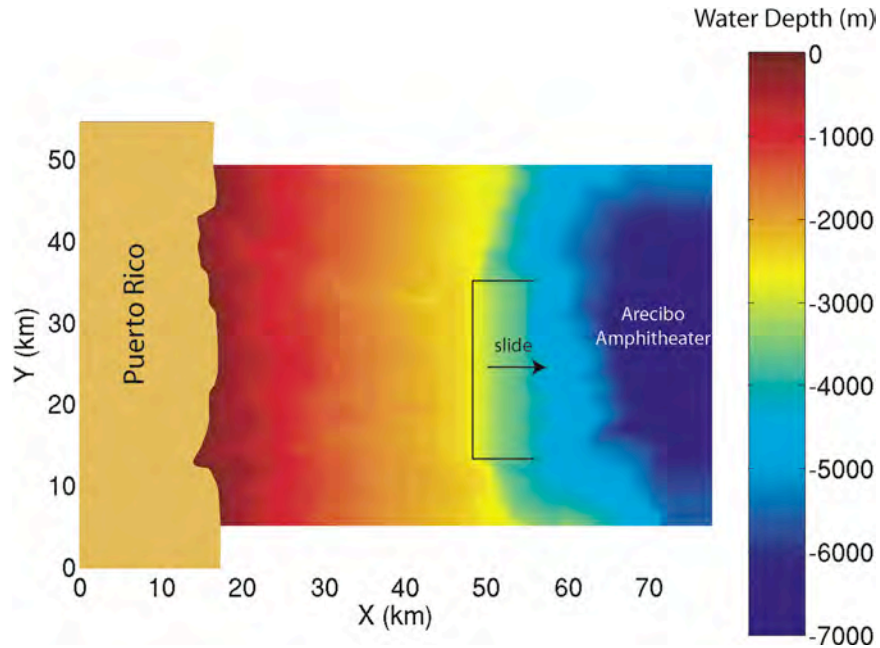


Figure 6. Bathymetry of part of the Arecibo amphitheater region along with a simple geometric representation of Arecibo slope failure A, interpreted from the multibeam bathymetry data (Figure 3a and c) and seismic profiles (Figure 4 d and e). Yellow region represents onshore Puerto Rico.

Slide movement is directly coupled with the hydrodynamic equations of motion through temporal and spatial derivatives of seafloor motion. As in *Mercado et al.*, (2002) hydrodynamic modeling is based on weakly nonlinear “extended” equations described by [*Lynett and Liu*, 2002]. Because of the large vertical motions associated with landslides, nonlinearity of the momentum equations may be more of a concern for landslide-generated tsunamis than for seismogenic tsunamis. When the maximum seafloor displacement is much smaller than the water depth above the slide, then the weakly nonlinear equations of [*Lynett and Liu*, 2002] can be used. Nonlinearity can also be important for accurately determining tsunami run-up, especially for large incident waves. As the tsunami propagates away from the source, frequency dispersion also becomes important. Landslide-generated waves are typically not the long waves characteristic of seismogenic sources, and so energy will be dispersed in the direction of wave propagation as different wave components (frequencies) travel at different velocities. Lynett and Liu (2002) use the arbitrary-level velocity computation [*Nwogu*, 1993] to “extend” the validity of frequency dispersion for the depth-integrated equations into the intermediate water regime, allowing for accurate simulation of waves with lengths greater than two water depths. The WNL-EXT equations are implemented in the program COULWAVE using a finite-difference approximation using a high-order predictor-corrector scheme. The spatial grid size used for the computations is 266 m with a time step of 0.51 s. In addition, bottom friction is accounted for with a constant friction factor $f=0.01$ (cf., *Mercado et al.*, 2002), using the quadratic bottom friction formulation. A moving boundary condition [*Lynett et al.*, 2002] is implemented along the coast to represent run-up and overland flow. For the open-ocean boundary conditions, a sponge-layer absorption scheme is used.

6. Hydrodynamic Results

Because Arecibo Slide A interpreted from the multibeam bathymetry is smaller in volume by nearly an order of magnitude than the large Arecibo amphitheater slide modeled by [*Mercado et al.*, 2002], the associated maximum run-up of Slide A is also necessarily smaller (20 m instead of 55 m, Figure 7). Figure 7a shows the wave field at $t=155$ s and the maximum wave amplitude for Slide A, for $t_d=133$ s. This duration time is smaller than the shortest duration time used by Mercado et al. (2002) for the much larger slide. It is reasonable to assume that the duration time scales with the dimensions of the slope failure. Similar plots for $t_d=200$ s and $t_d=400$ s are shown in Figures 7c-f, respectively, at the same scale as in Figures 7a and b. Increasing the slide duration dramatically decreases the maximum and near shore tsunami amplitude.

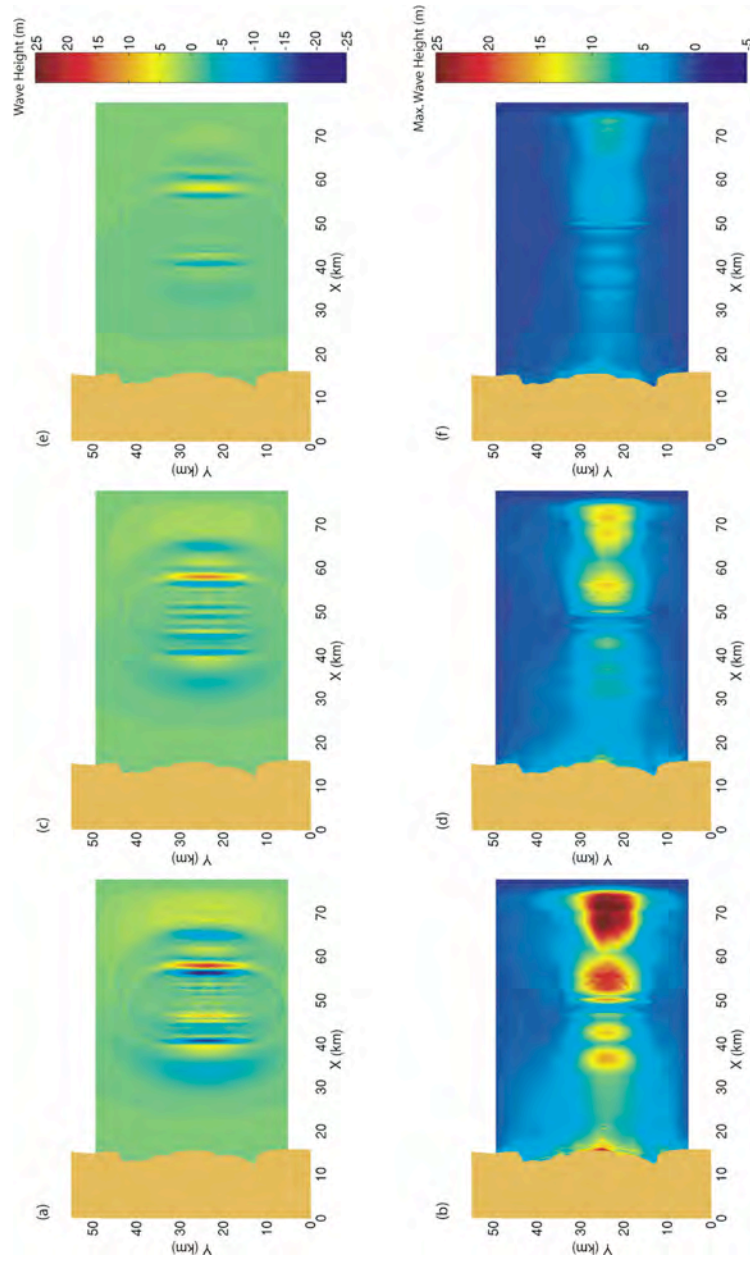


Figure 7. Hydrodynamic simulation for Slide A (Figure 6), using a slope failure duration $t_d=133$ s. (a) Wave field at $t=155$ s; (b) Maximum wave height for duration of model run (800 s). (c) Same as (a) for a failure duration of $t_d=200$ s. (d) same as (b) for a failure duration of $t_d=200$ s. (e) same as (a) for a failure duration of $t_d=400$ s. (f) same as (b) for a failure duration of $t_d=400$ s.

Because the slide is modeled as a region of progressive depletion and a down slope region of debris accumulation, it is difficult to assign an effective velocity for the slide as with simple block slides commonly used in tsunami studies (cf., [Ward, 2001]). Trifunac et al. (2003) describes composite slides of this type where different spreading velocities are assigned to the depletion and accumulation zones. In simpler, but perhaps less accurate terms, one can assign different length scales, such as run-out distance or horizontal displacement of the slide head, to calculate an effective velocity from t_d . Using 8 km characteristic length scale for Slide A and $t_d = 200$ s (Figure 7c), the effective slide velocity is approximately 40 m/s. This compares to a tsunami phase velocity ($c = \sqrt{gh}$ for long waves) of 170 m/s at a water depth of $h=3000$ m (approximate average water depth of the slide). For tsunamis propagating in the direction of slide motion (i.e., the outgoing tsunami), a slide velocity equal to the tsunami phase velocity is considered the ideal tuning velocity (Ward, 2001). As the duration decreases, the effective slide velocity is closer to the phase velocity and more efficient in terms of tsunami generation. For the tsunami propagating opposite the direction of slide motion (i.e., the incoming tsunami), generation efficacy follows a more complex relationship to both the initial acceleration of the slide and its terminal velocity. For the generation model used in this study, increasing the duration time does lead to a decrease in tsunami run-up on the near shore of Puerto Rico. We also examine the effect that a decrease in the friction factor f from $f=0.01$ to $f=0.001$ has on the maximum tsunami wave heights. A decrease in f results in a slight decrease in wave heights, similar to the effects noted by Mercado et al. [2002].

7. Recurrence time

An assessment of tsunami hazard assessment requires an estimate of recurrence time for slope failures. The absence of a historical record and clearly identified tsunami deposits on the northern coast of Puerto Rico, and the lack of dates on the observed slope failure, makes this task difficult. Nevertheless, the abundance of observed slope failures and hypotheses about the underlying causes of slope failures provide a starting point. A minimum recurrence time for slope failures along the edge of the carbonate platform was estimated assuming that the failure process was caused by the tilting of the platform at or after 3.3 m.y. ago, when the Puerto Rico trench collapsed and the island of Puerto Rico emerged (ten Brink, in press). We make the simplifying assumptions that slope failures were distributed evenly in time since the tilt event, and that the edge of the platform was initially straight (Figure 2b).

Unlike earthquakes, the size-frequency distribution of submarine slope failures is unknown. We therefore assume that the failures have a characteristic area and thickness similar to those observed. Three slope failure areas were calculated: Arecibo failure A with an area of 8x20 km, Loiza (future) failure B with an area of 3x15 km, and the Mona rift failure with an area of 4x20 km. Two other failures, Loiza failure A and Arecibo failure B are 22 and 15 km long, respectively, but their width is unknown. Based on the 3 calculated failure areas, the characteristic failure area along the edges of the carbonate platform is estimated to be 45-160 km². We take the number of large failures that occurred in the Arecibo and Loiza amphitheatres during the past 3.3 Ma to be the estimated lost area of carbonate platform divided by the characteristic failure area (Figure 2b). For the Arecibo Amphitheater, the estimated number of large failures is 7-25, and for the Loiza Amphitheater it is 4-13. The average recurrence time is therefore 470-132 ky for the Arecibo amphitheater and 825-253 ky for the Loiza amphitheater. The combined landslide tsunami recurrence interval at the north coast of Puerto Rico from the entire edge of the carbonate platform is 253-70 ky. This is probably a minimum estimate considering that there are other smaller failures which are probably capable of producing tsunamis.

Placement and configuration of turbidity layers can also help constrain the number of past slope failures within each amphitheater. Several events can be identified on the seismic profiles (Figure 4), but the resolution of these profiles is too poor to identify all the events. Additionally, some turbidity layers may be the result of massive sediment run-offs from the island after heavy storms, as represented in the backscatter images by the highly reflective channels coming down from the carbonate platform. A combination of near-bottom seismic reflection imaging and coring will help identify individual failure events.

8. Conclusions

Analysis of detailed multibeam bathymetry and coincident backscatter images from the edge of the carbonate platform north of Puerto Rico and the Virgin Islands combined with seismic cross-sections reveals numerous retrograde slope failures of various scales. Fissures, discovered in the ocean floor near the edge of the platform, indicate that the failure process is expected to continue in the future. The style of failure appears to be correlated with the presence of the carbonate layers at the headwall of the slide. Where the carbonate layer is thick, the failure often takes place as a rock fall or a rotated slump block perched on the lower slope, although debris avalanche or a debris flow may also take place. Secondary failure of the debris and of the exposed rocks that underlie the failed

carbonate platform may lead to additional slope failures, probably in the form of debris flows and turbidity flows. Because the primary sliding material is carbonate rocks, which are expected to fail in coherent rock masses, and because the edge of the carbonate platform is much steeper than many continental slopes around the U.S., slides off Puerto Rico may result in a higher potential run-up of tsunamis than comparable slides elsewhere. However, a few conterminous U.S. margins such as the Blake Escarpment and the lower slope of the New Jersey margin have composition and slope angle similar to those of Puerto Rico [Dillon et al., 1993], hence their failure mode may be analogous to our observations.

The 50-km wide escarpment, known as the Arecibo amphitheater, previously thought to have been formed by a single giant voluminous failure, is in effect the result of several slope failures. A hydrodynamic simulation using the weakly-nonlinear "extended" wave equations in the COULWAVE model, predicts a maximum run-up < 20 m on the northern coast of Puerto Rico from one of the slides at this place. This run-up amplitude is only 36% of the previously estimated run-up, which was calculated for the entire amphitheater sliding at once. The run-up is predicted to be even smaller for a longer sliding duration. A recurrence interval for the largest observed slope failures, such as the one modeled here is estimated using many simplifying assumptions to be between 100-800 ky. The lack of any established size-frequency relationship of submarine slope failures prevents us from extending this estimate to smaller failures.

Large submarine slides on the northern side of the Puerto Rico trench are found at greater depths (~ 6000 m), but can nevertheless be hazardous, because they aim toward Puerto Rico, have large horizontal and vertical dimensions and can excite lower frequency waves. These slope failures as well as a slide scarp discovered in the Upper Mona rift, possibly associated with the 1918 tsunami that hit northwestern Puerto Rico, should be further investigated.

This study demonstrates that high-resolution bathymetry, backscatter images, seismic profiles, and bottom samples, are necessary to evaluate the hazard from landslide tsunami. Emergency management cannot rely on tsunami warning for landslide tsunamis, because landslide tsunamis have short travel time from their source to the coast. Improved knowledge of the sea floor coupled with realistic simulations is needed to guide the preparation and mitigation of tsunami hazard.

The study was funded by NOAA Office of Ocean Exploration and the USGS Coastal and Marine Program and conducted aboard the NOAA ship Ronald

Brown, Shep Smith, Gene Parker, Toshi Uozumi, Bill Danforth, Chris Polloni, Brian Andrews, and Pilar Llanes were instrumental in collecting and processing the data. We thank Lisa Gahagan and the University of Texas seismic data center personnel for the seismic profiles. We thank David Twitchell, Jim Robb, and Tip Meckel for their constructive reviews.

References:

- Burroughs, S.M., and S.F. Tebbens, Power law scaling and probabilistic forecasting of tsunami runup heights, *Pure and Applied Geophysics*, 162, 331-342, 2005.
- Dillon, W.P., J. Acosta, A. Uchupi, and U.S. ten Brink, Joint Spanish-American research uncovers fracture pattern in northeastern Caribbean, *EOS*, 79, 336-337, 1998.
- Dillon, W.P., J.S. Risch, K.M. Scanlon, P.C. Valentine, and Q.J. Huggett, Ancient crustal fractures control the location and size of collapsed blocks at the Blake Escarpment, east of Florida, in *U. S. Geological Survey Bulletin, Report: B 2002*, edited by W.C. Schwab, H.J. Lee, and D.C. Twichell, pp. 54-59, 1993.
- Driscoll, N.W., J.K. Weisell, and J.A. Goff, Potential for large-scale submarine slope failure and tsunami generation along the U.S. Mid-Atlantic coast, *Geology*, 28, 407-410, 2000.
- Edwards, B.D., H.J. Lee, and M.E. Field, Seismically induced mudflow in Santa Barbara Basin, California, in *U. S. Geological Survey Bulletin, Report: B 2002*, edited by W.C. Schwab, H.J. Lee, and D.C. Twichell, pp. 167-175, 1993.
- Freeman-Lynde, R.P., and W.B.F. Ryan, Subsidence history of the Bahama Escarpment and the nature of the crust underlying the Bahamas, *Earth and Planetary Science Letters*, 84, 457-470, 1987.
- Grindlay, N.R., Volume and density approximations of material involved in debris avalanche on the south slope of the Puerto Rico Trench, *A report to the Puerto Rico civil Defense and the University of Puerto Rico Sea Grant College Program*, 9 pp, 1998.
- Grindlay, N.R., P. Mann, and J.F. Dolan, Researchers investigate submarine faults north of Puerto Rico, *EOS*, 78, 404, 1997.
- Heezen, B.C., and M. Ewing, Turbidity currents and submarine slumps, and the 1929 Grand Bank earthquake, *American journal of Science*, 250, 849-873, 1952.
- Hughes Clarke, J.E., Late stage slope failure in the wake of the 1929 Grand Banks earthquake, *Geo-Marine Letters*, 10, 69-79, 1990.
- Imamura, F., E. Gica, T. Takahashi, and N. Shuto, Numerical simulation of the

- 1992 Flores tsunami: Interpretation of tsunami phenomena in northeastern Flores Island and damage at Babi Island, *Pure and Applied Geophysics*, *144*, 555-567, 1995.
- Locat, J., H.J. Lee, P. Locat, and J. Imran, Numerical analysis of the mobility of the Palos Verdes debris avalanche, California, and its implication for the generation of tsunamis, *Marine Geology*, *203*, 269-280, 2004.
- Lynett, P., and P.L.-F. Liu, A Numerical Study of Submarine Landslide Generated Waves and Runup, *Proc. Royal Society of London A.*, *458*, 2885-2910, 2002.
- Lynett, P., T.-R. Wu, and P.L.-F. Liu, Modeling wave runup with depth-integrated equations, *Coastal Engineering*, *46*, 89-107, 2002.
- Ma, K.-F., H. Kanamori, and K. Satake, Mechanism of the 1975 Kalapana, Hawaii, earthquake inferred from tsunami data, *Journal of Geophysical Research*, *104*, 13,153-13,168, 1999.
- Mann, P., E. Calais, J.-C. Ruegg, C. DeMets, P.E. Jansma, and G.S. Mattioli, Oblique collision in the northeastern Caribbean from GPS measurements and geological observations, *Tectonics*, *21*, 1057, doi:10.1029/2001TC001304, 2002.
- Mercado, A., N.R. Grindlay, P. Lynett, and P.L.-F. Liu, Investigation of the potential tsunami hazard on the north coast of Puerto Rico due to submarine landslides along the Puerto Rico trench, *Report submitted to Puerto Rico State Emergency Management Agency and Sea Grant College Program*, 432, 2002.
- Mercado, A., and W. McCann, Numerical simulation of the 1918 Puerto Rico tsunami, *Natural Hazards*, *18*, 57-76, 1998.
- Monroe, W.H., Geology of the middle Tertiary formations of Puerto Rico, *U. S. Geological Survey Professional Paper*, *P593*, 93, 1980.
- Nwogu, O., Alternative form of Boussinesq equations for nearshore wave propagation, *Journal of Waterway, Port, Coastal, and Ocean Engineering*, *119*, 618-638, 1993.
- Piper, D.J.W., P. Cochonat, and M. L. Morrison, The sequence of events around the epicenter of the 1929 Grand Banks earthquake: initiation of debris flows and turbidity current inferred from sidescan sonar, *Sedimentology*, *46*, 79-97, 1999.
- Prior, D.B., and J.M. Coleman, Submarine slope instability, in *Slope instability*, edited by D. Brunsten, and D.B. Prior, pp. 419-455, Wiley and Sons, Chichester, 1984.
- Satake, K. and Y. Tanioka, The July 1998 Papua New Guinea earthquake: Mechanism and quantification of unusual tsunami generation, *Pure and Applied Geophysics*, *160*, 2087-2118, 2003.

- Scanlon, K.M., and D.G. Masson, Sedimentary processes in a tectonically active region: Puerto Rico North Insular Slope., in *Geology of the U.S. Seafloor: the View from GLORIA*, edited by J.V. Gardner, M. Field, and D.C. Twichell, pp. 123-134, Cambridge University Press, Cambridge, 1996.
- Schwab, W.C., W.W. Danforth, K.M. Scanlon, and D.G. Masson, A giant submarine slope failure on the northern insular slope of Puerto Rico, *Marine Geology*, *96*, 237-246, 1991.
- ten Brink, U.S., Vertical motions of the Puerto Rico Trench and their cause, *J. Geophys. Res.*, in press.
- ten Brink, U.S., W.W. danforth, C. Polloni, B. Andrews, P. Llanes, S.V. Smith, E. Parker, and T. Uozumi, New sea floor map of the Puerto Rico trench helps assess earthquake and tsunami hazards, *EOS*, *85*, 349, 354, 2004a.
- ten Brink, U.S., and J. Lin, Stress interaction between subduction earthquakes and forearc strike-slip faults: modeling and application to the northern Caribbean plate boundary, *Journal of Geophysical Research*, *109*, B12310, 10.1029/2004JB003031, 2004b.
- Trifunac, M.D., A. Hayir, and M.I. Todorovska, A note on tsunami caused by submarine slides and slumps spreading in one dimension with nonuniform displacement amplitudes, *Soil Dynamics and Earthquake Engineering*, *23*, 223-234, 2003.
- Twichell, D.C., P.C. Valentine, and L.M. Parson, Slope failure of carbonate sediment on the West Florida Slope, in *Submarine landslides: selected studies in the U.S. Exclusive Economic Zone*, edited by W.C.L. Schwab, H J; Twichell, D C, pp. 69-78, U. S. Geological Survey Bulletin, Report: B 2002, 1993.
- van Gestel, J.-P., P. Mann, J.F. Dolan, and N.R. Grindlay, Structure and tectonics of the upper Cenozoic Puerto Rico-Virgin Islands carbonate platform as determined from seismic reflection studies, *Journal of Geophysical Research*, *103*, 30,505-30,530, 1998.
- van Gestel, J.-P., P. Mann, N.R. Grindlay, and J.F. Dolan, Three-phase tectonic evolution of the northern margin of Puerto Rico as inferred from an integration of seismic reflection, well, and outcrop data, *Marine Geology*, *161* (2-4), 259-288, 1999.
- Varnes, D.J., Slope movement types and processes, in *Landslides: Analysis and Control*, edited by R. L Schuster and R. J. Krizek, pp. 11-33, National Academy of Sciences, Washington, D.C., 1978.
- Ward, S., Landslide tsunami, *Journal of Geophysical Research*, *106*, 11201-11215, 2001.
- Ward, S.N., and S. Day, Ritter Island Volcano; lateral collapse and the tsunami of 1888, *Geophysical Journal International*, *154*, 891-902, 2003.